

See discussions, stats, and author profiles for this publication at: <https://www.researchgate.net/publication/263167059>

Preparation and Mechanism Insight of Nuclear Envelope-Like Polymer Vesicles for Facile Loading of Biomacromolecules and Enhanced Biocatalytic Activity.

ARTICLE *in* ACS NANO · JUNE 2014

Impact Factor: 12.88 · DOI: 10.1021/nn502386j · Source: PubMed

CITATIONS

17

READS

35

4 AUTHORS, INCLUDING:



Cong Zhang

Tongji University

3 PUBLICATIONS 45 CITATIONS

[SEE PROFILE](#)



Jianzhong Du

Tongji University

68 PUBLICATIONS 2,841 CITATIONS

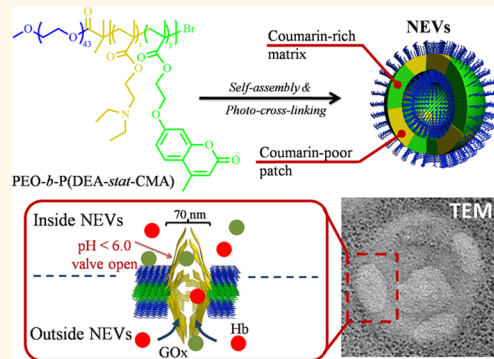
[SEE PROFILE](#)

Preparation and Mechanism Insight of Nuclear Envelope-like Polymer Vesicles for Facile Loading of Biomacromolecules and Enhanced Biocatalytic Activity

Yunqing Zhu, Fangyingkai Wang, Cong Zhang, and Jianzhong Du*

School of Materials Science and Engineering, Tongji University, 4800 Caoan Road, Shanghai, 201804, China

ABSTRACT The facile loading of sensitive and fragile biomacromolecules, such as glucose oxidase, hemoglobin, and ribonucleic acid (RNA), *via* synthetic vehicles directly in pure aqueous media is an important technical challenge. Inspired by the nucleus pore complex that connects the cell nucleus and the cytoplasm across the nuclear envelope, here we describe the development of a kind of polymeric nuclear envelope-like vesicle (NEV) to address this problem. The NEV is tailored to form the polymer pore complex (70 nm, similar to a nucleus pore complex) within the vesicle membrane based on nanophase segregation, which is confirmed *via* fluorescence spectrometry and dynamic light scattering (DLS) during self-assembly. This pH-triggered polymer pore complex can mediate the transportation of biomacromolecules across the vesicle membrane. Moreover, the NEVs facilitate the natural consecutive enzyme-catalyzed reactions *via* the H⁺ sponge effect. This simple strategy might also be extended for mimicking other synthetic cell organelles.



KEYWORDS: polymer vesicles · lateral segregation mechanism · nuclear envelope · biomacromolecule encapsulation · biocatalysis

The study on polymeric nuclear envelope-like vesicles (NEVs) will be important in biomedical applications considering that vesicles with membrane structure similar to nuclear envelopes can regulate either the transportation or the encapsulation of biomacromolecules under mild conditions. This is because the nucleus pore complex, scattered all around the nuclear envelope, is the only gateway connecting the cell nucleus and the cytoplasm in eukaryotes, which allows the free diffusion of small molecules and ions and mediates the transport of biomacromolecules, *e.g.*, proteins and RNAs.^{1–5} As a ring-like proteinaceous assembly, the nuclear pore complex has a pore diameter of about 45–70 nm, similar to the size of most biomacromolecules.^{6,7} Also, the attached filaments of the nucleus pore complex are critical for regulating the movement of biomacromolecules.^{8,9} However, the synthesis

of NEVs and their applications have not been previously reported.

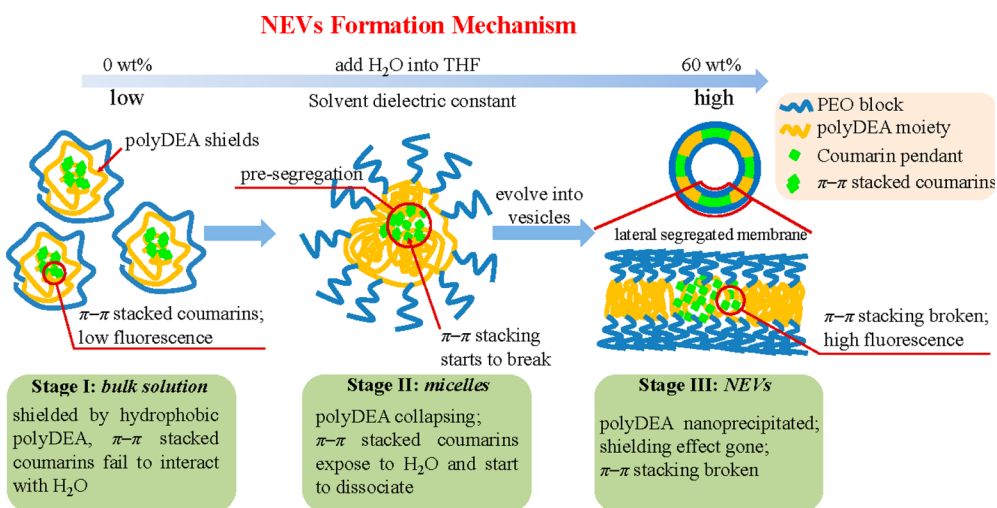
Since an amphiphilic polymer can self-assemble into a range of complex bioinspired nanostructures such as vesicles,^{10–16} it seems to be one of the best candidates for constructing nuclear envelope-like structures. Now, benefiting by their robust membrane and hollow structure, polymer vesicles are especially of great value in the transportation of small molecular compounds such as anticancer drugs^{17,18} or the encapsulation of certain catalysts to form nanoreactors.^{19,20} So far, (plant) viruses have been considered an effective vehicle for the encapsulation of functional enzymes.^{21,22} Although some biomacromolecules could be encapsulated by polymer vesicles during the self-assembly process in the presence of organic solvents (which may alter the structure of biomacromolecules) or using the film hydration method,^{23,24} it is not widely applicable for

* Address correspondence to
jzdu@tongji.edu.cn.

Received for review October 21, 2013
and accepted June 15, 2014.

Published online June 16, 2014
10.1021/nn502386j

© 2014 American Chemical Society



Scheme 1. Schematic self-assembly procedure of $\text{PEO}_{43}\text{-}b\text{-P}(\text{DEA}_{94}\text{-stat-CMA}_5)$ copolymer to form NEV. The coumarin pendant chains in the random coils of polymers form associates via $\pi-\pi$ stacking in THF (initial segregation) and are shielded by long hydrophobic polyDEA chains against high dielectric constant solvent, H_2O (stage I). With the collapsing of polyDEA, such associates start to dissociate upon the increasing of water content to form a micelle with PEO as the corona and $\text{P}(\text{DEA}_{94}\text{-stat-CMA}_5)$ as the presegregated core (stage II). The nanoprecipitation of polyDEA induces the full dissociation of $\pi-\pi$ stacking, leading to the formation of NEVs (stage III).

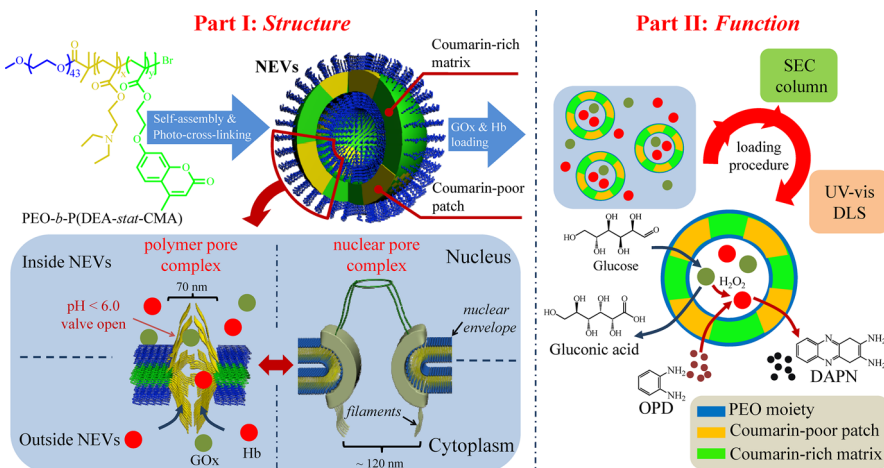
encapsulating those sensitive and fragile biomacromolecules for the preformed polymer vesicles in purely aqueous solution due to the lack of tunnels with suitable size in their membrane. Although there have been some pioneering works regarding polymer vesicles with controllable permeability for mediating the transportation of small molecules,^{25–27} and pH-sensitive encapsulation of various proteins through polyelectrolyte membranes has also been reported,^{28,29} the transportation of biomacromolecules with larger sizes within polymer vesicles remains a problem. Inspired by the nuclear envelope, which is inherent for efficiently transporting biomacromolecules, the investigation and biomimicking of nuclear envelope-like structures based on amphiphilic block copolymers may provide new insights for preparing advanced delivery vehicles for biomacromolecules, thus facilitating biocatalysis and even opening up the gate toward synthetic cells.

Herein, we propose a novel kind of nuclear envelope-like vesicle based on a pH-responsive and photo-cross-linkable diblock copolymer to face the challenge of facile transportation and encapsulation of biomacromolecules and mimicking consecutive enzyme-catalyzed reactions. The block copolymer is poly(ethylene oxide)-block-poly[2-(diethylamino)ethyl methacrylate]-stat-7-(2-methacryloyloxyethoxy)-4-methylcoumarin] [$\text{PEO}\text{-}b\text{-P}(\text{DEA}\text{-stat-CMA})$]. Different from the reactive $\text{PEO}\text{-}b\text{-P}(\text{DEA}\text{-stat-TMSPMA})$ copolymer, which is well known from the work of Armes and Du,³⁰ $\text{PEO}\text{-}b\text{-P}(\text{DEA}\text{-stat-CMA})$ block copolymer can form a more complex vesicle membrane due to $\pi-\pi$ stacking between poly-CMA. Mimicking the structure of the nucleus pore complex, the phase-separated polyDEA regions function as pH-manipulated valves in the vesicle membrane

because the hydrophilicity/hydrophobicity of polyDEA can be easily switched on/off by protonation/deprotonation. Also, protonated polyDEA chains can be partially regarded as polyelectrolyte filaments that project into both the cytoplasm and nucleoplasm from the nuclear pore complex as a selective barrier.³¹ Furthermore, photo-cross-linkable coumarin was introduced to prevent the disassociation of un-cross-linked NEVs upon dilution or environmental change (thermal effect, pH, etc.).³² It is also noteworthy that the coumarins can serve as both *in situ* photo-cross-linkable sites and fluorescence probes to monitor the “ $\pi-\pi$ stacking”-induced strong lateral segregation (Scheme 1).³³ As typical enzymes used in consecutive reactions, glucose oxidase (GOx) and hemoglobin (Hb, alternative for horse radish peroxidase) were encapsulated in NEVs. The loading mechanism and loading capability of NEVs (Scheme 2) were also evaluated. Thereafter, the consecutive enzyme-catalyzed reaction was mimicked using the enzyme-loaded NEVs to demonstrate the prompt elimination of the toxic intermediates (H_2O_2) during the glucose metabolic process. Furthermore, fluorescently labeled short interfering RNA (siRNA) was also encapsulated to demonstrate the generality of this encapsulation process.

RESULTS AND DISCUSSION

Design and Synthesis of Amphiphilic Block Copolymer. $\text{PEO}\text{-}b\text{-P}(\text{DEA}_{94}\text{-stat-CMA}_5)$ diblock copolymer with a very narrow molecular weight distribution ($M_n = 17\,700$ Da and $M_w/M_n = 1.04$ by GPC) was synthesized by atom transfer radical polymerization (ATRP). The synthesis and characterization of this copolymer are provided in Scheme S1, Figures S1–S5, and Table S1 in the Supporting Information.



Scheme 2. Formation of nuclear envelope-like vesicles (NEVs) and the encapsulation of biomacromolecules for biocatalyzed consecutive reactions. **Part I:** Inspired by the structure of a natural nuclear pore complex, the PEO-*b*-P(DEA-*stat*-CMA) diblock copolymer forms NEVs, consisting of a coumarin-rich matrix (green continuous phase, containing both coumarins and DEAs due to random copolymerization) and coumarin-poor patches (yellow discontinuous phase mainly consisting of DEA moieties; owing to the phase separation, coumarin-poor patches serve as giant valves, polyelectrolyte filaments, and proton sponge). The coumarin-rich matrix can be easily cross-linked upon UV radiation. The giant valves (yellow) can open and close by tuning the pH, favoring the encapsulation of various biomacromolecules, such as glucose oxidase (GOx, dark green balls) and hemoglobin (Hb, red balls). Please note that although the valve (yellow) is rich in DEA, it is not fully perforated due to the existence of a very small fraction of coumarin in this region (not shown in this scheme), which makes this polymer pore complex very similar to the nucleus pore complex. **Part II:** Purified by size exclusion chromatography (SEC) and characterized by UV-vis and dynamic light scattering (DLS), the glucose oxidase and hemoglobin-loaded NEVs were proven to be an excellent nanoreactor for biocatalyzed consecutive reactions.

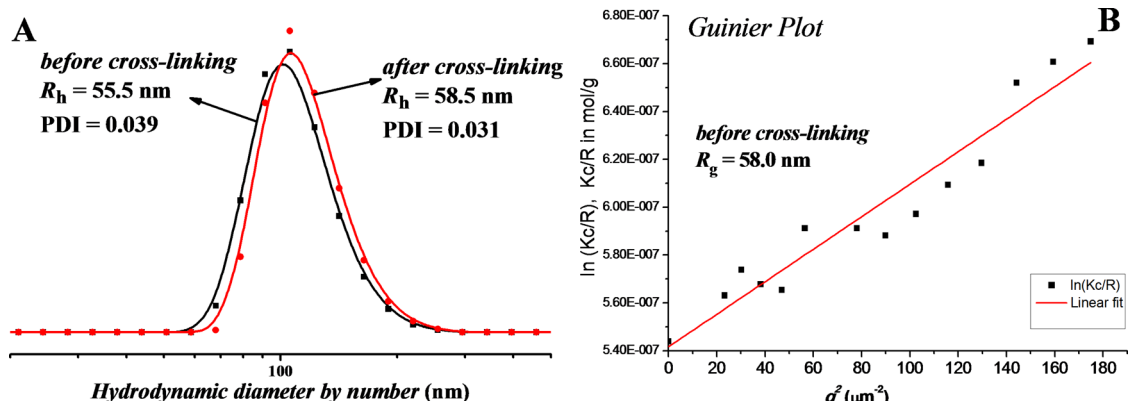
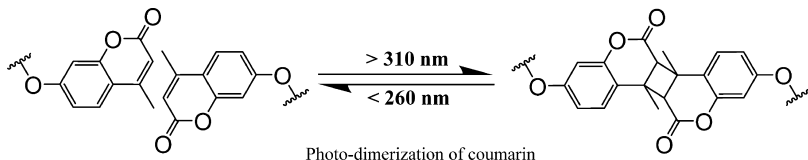


Figure 1. Dynamic and static light scattering analyses of PEO-*b*-P(DEA₉₄-*stat*-CMA₅) vesicles: (A) hydrodynamic radius (R_h) and near monodispersity of vesicles determined by DLS both before and after photo-cross-linking; (B) Guinier plot and radius of gyration (R_g) of un-cross-linked vesicles determined by SLS.

Self-Assembly of PEO-*b*-P(DEA₉₄-*stat*-CMA₅) to Vesicles. The NEVs were easily formed by self-assembly of PEO-*b*-P(DEA₉₄-*stat*-CMA₅) block copolymer in the mixture solvent of THF/water (1:2, v/v) at an initial copolymer concentration (C_{ini}) of 6.80 mg/mL in THF. Usually, the particle morphology is predictable by evaluating its R_g/R_h value.³⁴ Here, R_g is the radius of gyration determined by static light scattering (SLS) and R_h is the hydrodynamic radius determined by dynamic light scattering (DLS). For instance, an R_g/R_h of 0.774 implies a solid sphere, while 1.00 represents a thin-layer hollow structure (e.g., vesicle). As expected, the R_g and R_h values were measured to be 58.0 and 55.5 nm, respectively, indicating a vesicular structure with an R_g/R_h value of 1.04. Moreover, the polydispersity index (PDI) of 0.039

determined by DLS indicated a near monodispersity ($\mu_2/\Gamma^2 < 0.05$).^{35,36}

Transmission electron microscopy (TEM) was used to reveal the morphology of un-cross-linked vesicles. Due to the relatively low contrast of polymer vesicles, the TEM sample was stained by phosphotungstic acid (PTA). As shown in Figure S6 in the Supporting Information, the average diameter of the polymer vesicles was ~100 nm, which is consistent with the DLS and SLS results in Figure 1. The high contrast small dots appearing in the TEM image are the residual staining agent. The membrane thickness is roughly estimated to be ~10 nm. Meanwhile, a slight lateral segregation was also observed in Figure S6.



Scheme 3. Photodimerization process of coumarins.

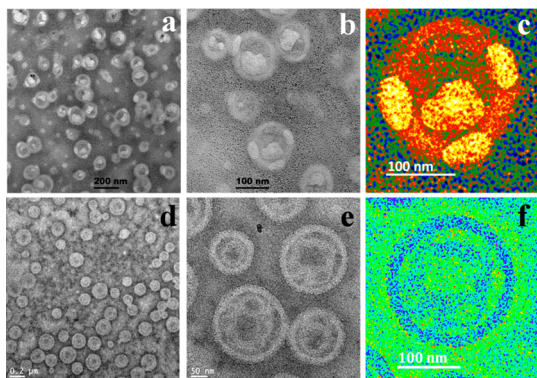


Figure 2. TEM images of cross-linked NEVs without any staining: (a and b) TEM image of NEVs with strong lateral segregation. The bright patches are coumarin-poor regions surrounded by a high-contrast matrix, coumarin-rich region. (c) Inverse fast Fourier transform (IFFT) image of a single NEV; (d and e) TEM images of NEVs decorated by AuNPs. The contrast reversed to high-contrast patches (corresponding to high AuNP content in the coumarin-poor region) and a low-contrast matrix (corresponding to low AuNP content in the coumarin-rich region). (f) IFFT image of a single AuNP-decorated NEV.

Photo-Cross-Linking of NEVs. The hydrophilic PEO chains form the coronas, whereas the hydrophobic P(DEA-stat-CMA) block forms the phase-separated vesicle membrane because of the hydrophobic effect of polyDEA and the $\pi-\pi$ stacking effect of coumarin moieties during the self-assembly process. Coumarin compounds undergo photodimerization upon UV irradiation ($\lambda \approx 365$ nm) to afford interchain covalent bonds (Scheme 3). Therefore, to stabilize the vesicular structure and to enhance the lateral segregation, the polymer vesicles were photo-cross-linked (see Methods section for detailed procedure and the calculation of dimerization degree). Monitored by DLS, both the hydrodynamic diameter (D_h) and the PDI of the vesicles barely changed during the photo-cross-linking period (Figure S7B in the Supporting Information), suggesting a high colloidal stability of NEVs and no intervesicle cross-linking. The dimerization degree of the coumarin increased rapidly and reached a maximum degree of 76% after 120 s, indicating that the cross-linking degree is controllable by tuning the UV exposure time.

Morphology Study of NEVs after Photo-Cross-Linking. TEM was used to probe the NEVs' structure directly after photo-cross-linking without staining. As demonstrated in Figure 2a and b, NEVs with an obvious laterally segregated membrane were observed: low-contrast patches (nonconsecutive regions embedded in the NEVs' membrane) were surrounded by a high-contrast

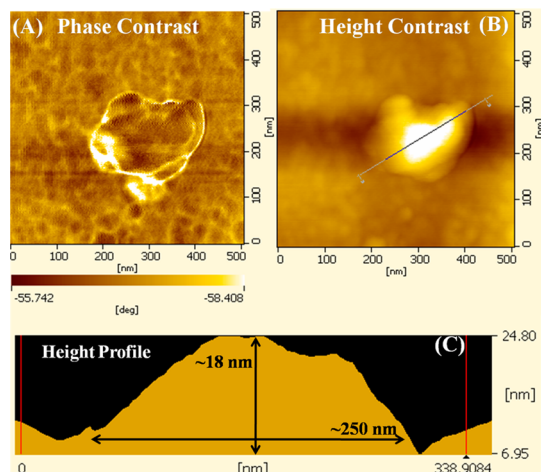


Figure 3. AFM images of PEO₄₃-b-P(DEA₉₄-stat-CMA₅) vesicles: (A) phase contrast demonstrates slight phase separation, and the irregular shape indicates different rigidity of segregated phases; (B) height contrast; (C) section profile of the AFM image along with the scan line in (B). The diameter/height ratio is in agreement with a hollow structure.

matrix (continuous phase in the NEVs' membrane). Colored inverse fast Fourier transform (IFFT) technique was adopted to enhance the contrast of TEM images (Figure 2c). As the contrast ratio of TEM images is simply the reflection of electron transmittance,³⁷ the benzene-like structure with large π bonds usually has a lower electron transmittance (high contrast). Therefore, low-contrast patches (calculated mean size of ~ 70 nm, the same size as the nucleus pores) located in the NEVs' membrane were assumed to be coumarin-poor regions mainly consisting of polyDEA moieties, while the high-contrast matrix acting as a skeleton in the NEVs' membrane is believed to be highly cross-linked coumarin-rich regions [please note that polyDEA is also partially contained in this region due to the architecture of statistical copolymer].

To reveal the subtle nanostructure of polymer vesicles, atomic force microscopy (AFM) was employed, which was conducted at mild conditions to prevent damage of the soft samples. AFM analysis evidenced a high diameter/height ratio (250 nm/18 nm, Figure 3C), which is characteristic for collapsed vesicles,³⁸ and the membrane thickness of ca. 9 nm is also in good agreement with that determined by TEM (around 10 nm).

In addition, different from normal vesicles, the phase contrast AFM image confirms the slight phase segregation within the vesicle membrane (Figure 3A) and an irregular shape caused by the different rigidity of phases.

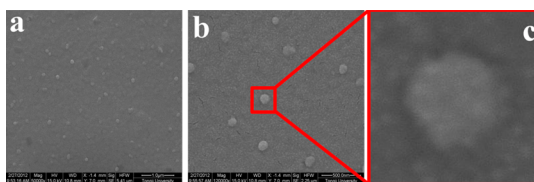


Figure 4. SEM images of NEVs. An enlarged NEV in (c) verifies that the patches appearing in the TEM images are phase-segregated membrane regions rather than macropores.

Moreover, to rule out the possibility that the low-contrast patches might be macropores instead of coumarin-poor regions, the surface morphology of NEVs was investigated *via* scanning electron microscopy (SEM). As shown in Figure 4, the smooth surface of NEVs clearly eliminates the possibility that those low-contrast patches were macropores.

On the basis of the TEM, AFM, and SEM analyses, we think that although slight phase segregation takes place before cross-linking, the photodimerization between coumarin moieties further promotes the phase separation of the vesicle membrane (Figure 2a–c).

To further verify the assumption of a patch-forming DEA-rich (coumarin-poor) phase and a matrix-forming coumarin-rich phase, the gold nanoparticle (AuNP) decoration method³⁰ was chosen to selectively “stain” the DEA-rich (coumarin-poor) region between both regions. As expected, a similar lateral segregation morphology of AuNP-decorated NEVs was observed by TEM (Figure 2d,e). Both the TEM images and colored IFFT image (Figure 2e,f) revealed a totally contrary contrast code to the NEVs without AuNPs (Figure 2a–c): low-contrast matrix and high-contrast patches. These interesting contrast switches of patch and matrix on the NEVs' membrane resulted from the selective “staining” of AuNPs of coumarin-poor regions and evidently supported our theory concerning the lateral segregation of coumarin-poor and coumarin-rich phases.

By now, TEM, AFM, light scattering, and SEM have certainly confirmed the strong lateral segregation morphology of NEVs. How do the simple block copolymer chains form such complex NEVs? Considering that the polyDEA chains become solvophobic at high water content and the coumarins form $\pi-\pi$ stacking, we supposed that the synergic mechanism between the increasing solvophobicity of polyDEA and the dissociation of the preformed $\pi-\pi$ stacking^{39,40} of the coumarins during self-assembly (*e.g.*, from pure THF to a THF/water mixture) is the main driving force of lateral segregation, as discussed below.

Mechanism Insight: How Does a Hydrophobic Block Afford a Lateral Segregated Membrane? To justify the above formation mechanism of NEVs, we designed the following fluorescence and DLS experiments: (1) Monitoring the fluorescence intensities during the formation process of the NEVs using coumarin pendants in the copolymer

as the internal fluorescence probes. In a parallel experiment, the fluorescence intensities of the coumarin monomer (CMA) were also monitored for comparison. These experiments will reveal the $\pi-\pi$ stacking degree because coumarins are relatively water-soluble compounds at millimolar (mM) level and undergo fluorescence quenching when locally concentrated or forming $\pi-\pi$ stacking.^{41,42} (2) Tracing the self-assembly process by DLS, which indicates the corresponding morphologies of the particles. In the above experiments, DI water was added dropwise into the THF solution of the PEO₄₃-*b*-P(DEA₉₄-stat-CMA₅) block copolymer to induce the formation of NEVs. During that period, aliquots were withdrawn for both fluorescence and DLS analyses, with equivalent coumarin monomer as reference.

As the reference, the fluorescence intensity of the coumarin monomer solution increases with the increase of water content, resulting from the disassociation of originally $\pi-\pi$ stacked coumarins in THF upon enhanced dielectric constant by adding water (Figure 5A). However, as for the PEO-*b*-P(DEA₉₄-stat-CMA₅) diblock copolymer, the fluorescence intensity experienced three stages, and similar behavior was observed in the variation of the hydrodynamic diameter (D_h) determined by DLS as well (Figure 5B). The symbiotic relationship between the disassociation of the coumarin $\pi-\pi$ stacking and self-assembly can be explained by the three-stage self-assembly mechanism (Scheme 1). Stage I (water content <39 wt %): screened by long hydrophobic DEA chains, $\pi-\pi$ stacked coumarins failed to interact with water molecules to disassociate, leading to a weak fluorescence emission. Stage II (water content around 42 wt %): hydrophobic DEA segments started to collapse and aggregate, leaving $\pi-\pi$ stacked coumarins exposed to water molecules, and disassociated, thus resulting in the startup of the fluorescence intensity rising. Stage III (water content >45 wt %): the nanoprecipitated DEA segments and the fully disassociated coumarins form the laterally segregated membrane structure of NEVs, as evidenced by coumarin-poor patches and a coumarin-rich matrix by TEM.

pH Sensitivity of NEVs. The pH sensitivity of NEVs was studied first to explore the possibility of biomacromolecule encapsulation through coumarin-poor patches (pH-controlling valves) in purely aqueous solution, which is similar to a nucleus pore complex. To eliminate the interference of dilution on NEVs' size during pH tuning, an un-cross-linked NEV solution was diluted 16-fold. No noteworthy change in both hydrodynamic diameter and polydispersity index was observed (Figure S9), implying dilution scarcely affects the morphology of NEVs. As shown in Figure 6A, before cross-linking the D_h depends on pH: at pH > 6.0, both D_h and PDI are nearly constant because the tertiary amine stayed hydrophobic; at pH < 6.0, the tertiary

amines were protonated, resulting in the swelling of NEVs and an increase in PDI. However, after cross-linking (Figure 6B), although the D_h is still affected by

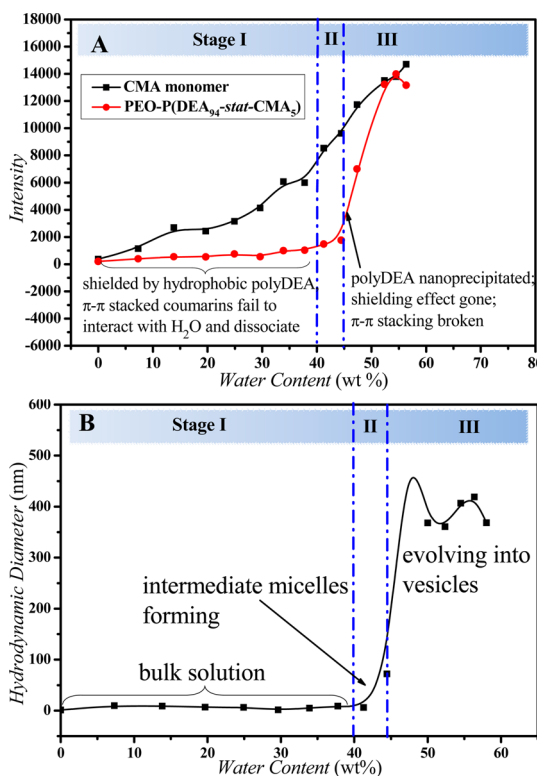


Figure 5. Three-stage formation mechanism of a nuclear envelope-like vesicle (NEV) justified by two independent fluorescence and DLS experiments: (A) Fluorescence intensities of the CMA monomer (■) and CMA containing a diblock copolymer (●). The three-stage increasing process of the copolymer (●) indicates a sudden change in the surrounding environment of the CMA pendant, which is NOT observed in the sample of merely the CMA monomer (■); (B) the relationship between the hydrodynamic diameter and water content of the PEO-*b*-P(DEA₉₄-stat-CMA₅) diblock copolymer during the self-assembly procedure. Similar to the fluorescence study, DLS results also undergo a transition at the water content around 42 wt %, which means the sudden jump in the fluorescence intensity of copolymer (●) is caused by the formation of micelles.

pH (increasing from 150 to 220 nm) because of the solvated coumarin-poor patches, the PDI stays constant, exhibiting high colloidal stability even at pH 2.5. As the skeleton, the cross-linked coumarin-rich matrix contributed to the significant stability, while coumarin-poor patches functioned as a pH-triggered tunnel. Usually, cross-linked self-assembly is considered as a suitable vehicle for compounds with low molecular weight. Nevertheless, this NEV makes the packing and delivery of high molecular weight compounds possible, such as protein, RNA, and polysaccharide.

Encapsulation of Biomacromolecules into NEVs. As we mentioned before, most reported self-assembly encapsulation techniques for biomacromolecules are either too complex for application⁴³ or incompatible for those sensitive and fragile biomacromolecules, such as the widely used solvent switch method.²³ Recently, Armes *et al.* exploited an approach to address this problem.⁴⁴ By temporarily destabilizing the vesicle membrane *via* electroporation, biomacromolecules (such as BSA) can be encapsulated by polymer vesicles. However, polymeric vesicles are somewhat too stable for electroporation compared with liposomes. Therefore, the parameters such as voltage, pulses, duration, frequency, and the solution properties can seriously affect the membrane permeabilization.^{45,46}

Our NEVs have excellent water-dispersibility, mild loading conditions for biomacromolecules in purely aqueous media, high colloidal stability, multifunctions (AuNP decoration, pH-responsive drug and biomacromolecule delivery, and biocatalysis), and especially the same pore size as a nucleus pore complex, which are thus tailored to conquer those challenges such as the facile encapsulation of those sensitive and fragile biomacromolecules in pure water. Glucose oxidase (D_h by DLS: ca. 17.4 nm) and hemoglobin (D_h by DLS: ca. 6.0 nm), exhibiting great catalyzing ability,^{47–49} were encapsulated in NEVs *via* tuning the pH between 5.5 and 6.5 without the aid of any organic solvents (relative zeta potential data are listed in Table S2; see

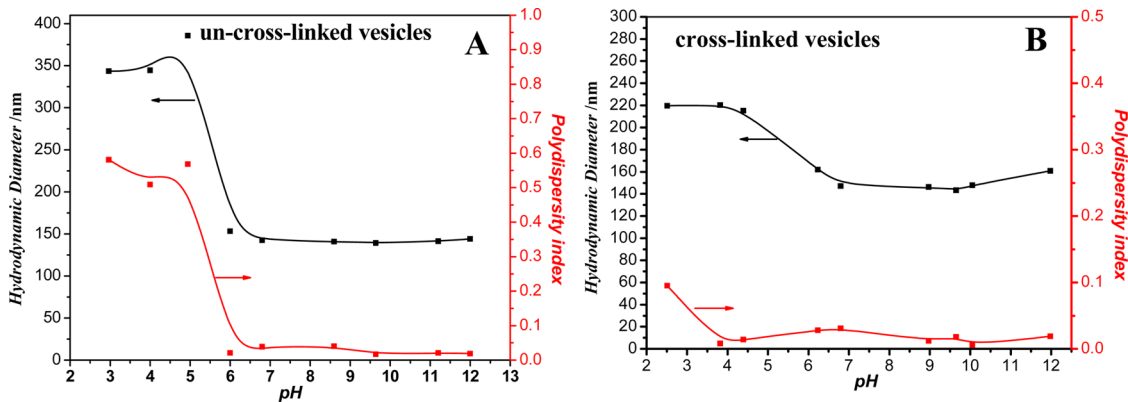


Figure 6. pH-responsive behavior of NEVs: (A) Un-cross-linked vesicles. Both D_h and PDI increase dramatically in acidic water from ca. 150 nm to ca. 350 nm and from 0.019 to 0.581, respectively. (B) Cross-linked vesicles. The D_h experiences a slight increase and the PDI remains low (<0.1).

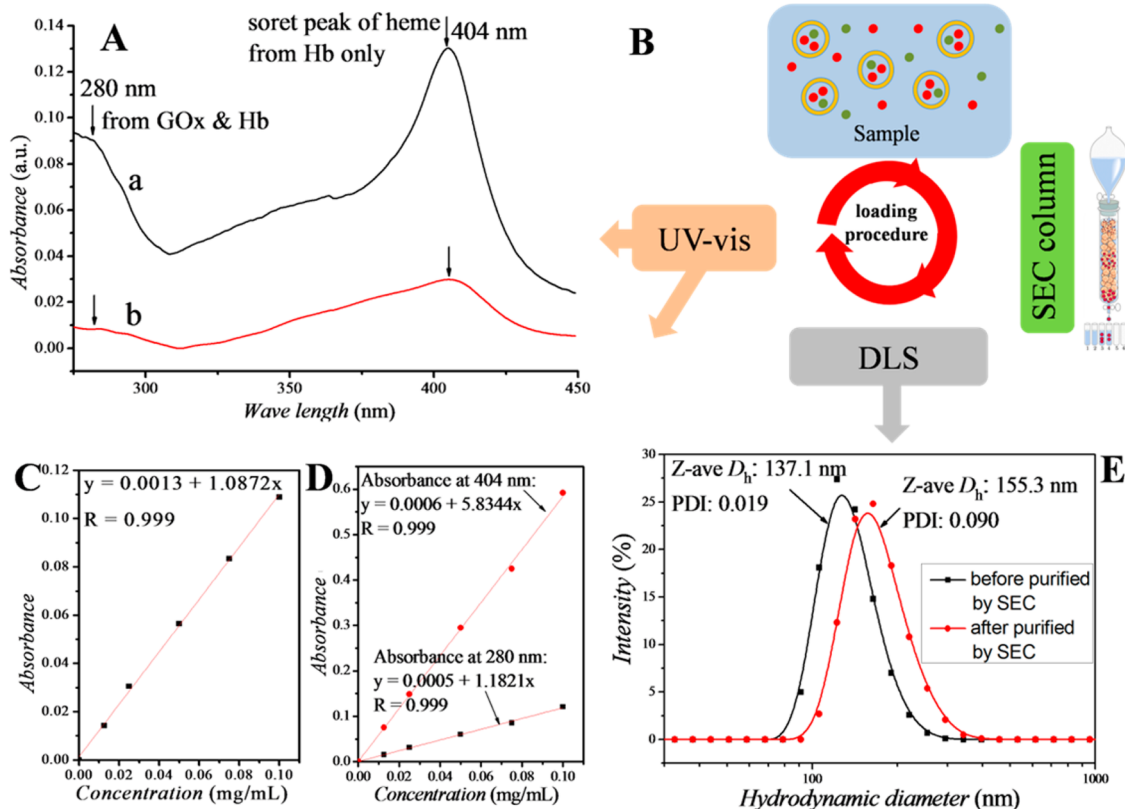
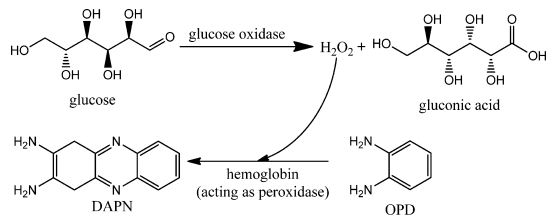


Figure 7. Schematic procedure of GOx and Hb encapsulation into NEVs. (A) UV-vis spectra of GOx and Hb: sample was prepared by tuning the pH (curve a) and without tuning the pH (curve b, control experiment). The absorption at 404 nm represents the Soret absorbance peak of heme in hemoglobin, and the absorption at 280 nm belongs to the amino acid residue of both glucose oxidase (GOx) and hemoglobin (Hb). (B) Schematic enzyme-loading procedure: first incubated with NEVs, then purified via SEC and characterized by DLS and UV-vis. (C) Calibration curve of glucose oxidase at 280 nm in DI water. (D) Calibration curve of hemoglobin at both 280 and 404 nm in DI water. (E) DLS measurement of NEVs before (■) and after (●) purification via SEC; the eluent with the DLS signal similar to pure NEVs was collected as the (GOx and Hb)-loaded NEVs.

Methods section for detailed encapsulation process). The NEVs' size, concentration of biomacromolecules, and biomacromolecule-loading efficiency (BLE) were evaluated and calculated by DLS and UV-vis spectroscopy (see Figure 7). The loading efficiencies of GOx and Hb were calculated to be 14.3% and 18.7%, respectively, according to the UV-vis calibration curve (Figure 7C and D). Also, a control experiment was conducted without pH tuning, and no hemoglobin absorbance can be observed in the UV-vis spectrum, confirming that GOx and Hb were encapsulated inside NEVs rather than physically adsorbed. Thus, biomacromolecules with similar size such as BSA, IgG, siRNA, pDNA, Mb, and Lz could also be encapsulated into NEVs.

To demonstrate the generality of the encapsulation process, the encapsulation of fluorescently labeled siRNA (FAM-siRNA) was also conducted. The loading efficiency was calculated to be 12.4% using the fluorescent emission band of the FAM at 525 nm (see Figure S10 for the calibration curve and fluorescence spectrum).

GOx and Hb-Loaded NEVs for Biocatalysis. Biocatalyst (GOx and Hb)-loaded NEVs were examined by consecutive oxidation reactions: glucose forming gluconic



Scheme 4. Consecutive enzyme-catalyzed reactions by glucose oxidase and hemoglobin.

acid and H_2O_2 ; *o*-phenylenediamine (OPD) forming 2,3-diaminophenazine (DAPN) (see Scheme 2 and Scheme 4).⁵⁰ As displayed in Figure 8, the absorbance of samples c, d, and e (pure Hb, pure NEVs, and pure GOx, respectively) barely changed in 30 min (Figure 8 inset), while the ones of samples a and b increased rapidly over the reaction time. However, in comparison to sample a (GOx and Hb-loaded NEVs), sample b (free GOx and Hb) demonstrated a relatively faster reaction rate for OPD at the beginning, yet slowed after 12 min. Interestingly, after 20 min, the extent of the reaction in sample a exceeded that in sample b (red circle in Figure 8), which we assumed to be the consequence of pH variation. Since gluconic acid can dramatically

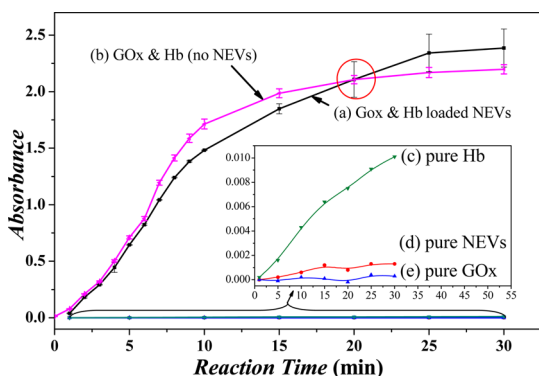


Figure 8. Mimicking biocatalysis in the nuclear envelope-like vesicle (NEV): UV-vis absorbance of 2,3-diaminophenazine (DAPN), the product of *o*-phenylenediamine (OPD) oxidation, against reaction time in the presence of OPD, glucose, and (a) GOx and Hb-loaded NEVs; (b) free GOx and Hb; (c) pure Hb; (d) pure NEVs; (e) pure GOx. Corresponding concentrations in the final mixture: OPD (0.247 mg/mL), NEVs (0.184 mg/mL), glucose (1.06 mg/mL), hemoglobin (0.011 mg/mL), glucose oxidase (0.023 mg/mL). Inset: Enlarged OPD oxidation process with only Hb, NEVs, and GOx, respectively.

reduce the pH of the reaction system and Hb denatures to a considerable extent at pH < 4.0,⁵¹ the pH value is crucial during the consecutive reactions. After 30 min of UV-vis monitoring, the pH values of samples a (with NEVs) and b (without NEVs) were measured to be 4.6 and 3.8, respectively, confirming that the different reaction rates in the OPD oxidation between samples a and b result from pH variation.

We believe the pH difference is caused by the polyDEA from NEVs, acting as the “proton sponge” (buffer solution) and in the meantime facilitating the

consecutive reaction of glucose. It is noteworthy that under such low pH those pores will inevitably open, which might jeopardize encapsulation. However, those polymer complex pores contain protonated polyDEA chains. Therefore, the transportation of biomacromolecules through those pores is slow, as the pore is not entirely open without any hindrance; that is why the encapsulation process took 2 days. Considering that the catalytic process requires merely 30 min, which is only 1/96 (ca. 1%) relative to the encapsulation process, it is reasonable to believe those enzymes remain encapsulated during the experimental period.

CONCLUSIONS

In summary, we have shown that the specially designed polymeric nuclear envelope-like vesicles could nondestructively and efficiently encapsulate sensitive and fragile biomacromolecules such as proteins and RNAs in pure aqueous solution triggered by slight pH changes. This facile loading method is applicable for a range of biomacromolecules due to polymer pore complex scattering all over the vesicle membrane, which is similar to the nucleus pore complex. Furthermore, we have confirmed that, after being encapsulated in NEVs, GOx and Hb still exhibited enhanced biocatalysis activity in the consecutive enzyme-catalyzed reactions. If applied successfully, NEVs would be significant innovations in encapsulating biomacromolecules in polymer vesicles directly in water and might also be applicable for small nanoparticles, leading to diverse and endless biomedical applications especially for gene therapy.

METHODS

Materials. 7-Hydroxy-4-methylcoumarin, 2-bromoethanol, methacryloyl chloride, and α -bromoisobutyryl bromide was purchased from Aladdin Chemistry, Co. Potassium carbonate, NaOH, NaCl, MgSO₄, Cu(II)Br, triethylamine (TEA), acetone, dichloromethane, tetrahydrofuran (THF), and other solvents were purchased from Sinopharm Chemical Reagent Co., Ltd. (SCRC, Shanghai, China) and used as received. *N,N,N',N'',N'''-Pentamethylidihylenetriamine* (PMDETA) and 2-(diethylamino)ethyl methacrylate (DEA) were purchased from Sigma-Aldrich. The DEA monomer was passed through an alumina B column to remove the inhibitor before use. Dialysis tubing (8–14 kDa molecular weight cutoff) was supplied by Shanghai Genestar Bio-Technology Co., Ltd. Poly(ethylene glycol) methyl ether (MeO-PEO-OH; M_n ca. 1900 Da; M_w/M_n = 1.10) was purchased from Alfa Aesar (Tianjin) Chemistry Ltd. CDCl₃ was purchased from J&K Scientific Ltd. Before use, 7-hydroxy-4-methylcoumarin was recrystallized from ethanol and stored at room temperature; THF was dried using metallic sodium and distilled; Cu(II)Br was stirred in glacial acetic acid for 5 h, then washed with acetone six times and stored with argon protection. Hemoglobin and glucose oxidase were purchased from Aladdin Chemistry, Co. FAM-labeled siRNA (13.3 kDa) was supplied by Genepharma.

Characterization. **GPC.** The molecular weights and polydispersities of PEO-*b*-P(DEA-stat-CMA) were characterized using a THF GPC conducted by a Waters Breeze 1525 GPC analysis system with two PL mixed-D columns with HPLC-grade THF as the eluent at a flow rate of 1.0 mL/min at 35 °C.

PEO-*b*-P(DEA-stat-CMA) was dissolved in THF and filtered prior to analysis. THF GPC analysis (refractive index detector) gave M_n = 17 700 Da and M_w/M_n = 1.05 (see Figure S5) using a series of near-monodisperse polystyrene calibration standards.

¹H NMR. ¹H NMR spectra were recorded using a Bruker AV 400 MHz spectrometer at room temperature with CDCl₃ as solvent.

DLS. Dynamic light scattering was used to determine the hydrodynamic radius (R_h) and polydispersity of NEVs in aqueous solution. The hydrodynamic diameters of NEVs were characterized by a ZETASIZER Nano series instrument (Malvern Instruments ZS 90). The scattering angle was fixed at 90°. Data processing was carried out using cumulant analysis of the experimental correlation function and analyzed using the Stokes-Einstein equation to calculate the hydrodynamic diameters of NEVs. Viscosity and refractive index were linearly calculated from pure water and THF as the solvent properties for the DLS characterization.

SLS. Static light scattering was used to determine the radius of gyration and was conducted using ALV/5000E laser light scattering. The data were analyzed using the Guiner plot method on ALV software to determine R_g .

UV-Vis Spectroscopy. UV-vis spectroscopy of the photo-cross-linking process and redox reaction catalyzed by GOx and Hb-loaded NEVs was acquired using a UV7595 UV-vis spectrophotometer (Shanghai Precision and Scientific Instrument Co., Ltd.). All samples were analyzed using quartz cuvettes with a path length of 10 mm.

TEM. All vesicle solutions were diluted at ambient temperature. Copper grids were surface-coated to form a thin layer of amorphous carbon. Each sample ($4\text{ }\mu\text{L}$) was then dropped onto the carbon-coated grid and dried at ambient environment with or without staining. The cross-linked vesicles were viewed without staining. However, the un-cross-linked vesicles were stained by phosphotungstic acid solution (PTA) because it is difficult to visualize the samples. To stain the un-cross-linked vesicles, $10\text{ }\mu\text{L}$ of PTA (2 w/w %, tuned to neutral pH using 1.0 M NaOH solution) was dropped onto a hydrophobic film (Parafilm); then those sample-loaded grids were laid upside down on top of the PTA solution droplet and soaked for 1 min. After that a filter paper was used to carefully blot the excess PTA solution. The grids were dried under ambient environment overnight. Imaging was recorded on a JEOL JEM-2100F instrument at 200 kV equipped with a Gatan 894 Ultrascan 1k CCD camera.

AFM. AFM was employed to verify the hollow structure (height contrast) and strong lateral segregation (phase contrast) of NEVs. An NEV solution was diluted at ambient temperature, dropped ($10\text{ }\mu\text{L}$) onto the silicon wafer ($1 \times 1\text{ cm}^2$), and dried at room temperature. The silicon wafer was washed with acetone four times before sample preparation. The observation was conducted on a Seiko (SPA-300HV) instrument operating in tapping mode at 200–400 kHz drive frequency.

SEM. SEM was utilized to observe the surface morphologies of NEVs. To obtain SEM images, a drop of solution was spread on a silicon wafer and left until dryness. It was coated with platinum and viewed by an FEI Quanta 200 FEG electron microscope operated at 15 kV. The images were recorded by a digital camera.

Fluorescence Spectroscopy. Fluorescent experiments were carried out to monitor the self-assembly procedure of PEO-*b*-P(DEA-stat-CMA) with CMA as internal probe ($\lambda_{\text{ex}} = 320\text{ nm}$, $\lambda_{\text{em}} = 367\text{ nm}$) via a Lumina fluorescence spectrometer (ThermoFisher).

Zeta Potential. Zeta potential studies were conducted at $25\text{ }^\circ\text{C}$ using a ZETASIZER Nano series instrument (Malvern Instruments) for measuring the zeta potential of NEV glucose oxidase and hemoglobin solutions at different pH values.

Synthesis of Macroinitiator (PEO-Br). The PEO-Br macroinitiator was prepared via the reaction of MeO-PEO-OH with excess 2-bromoisobutryl bromide as reported before.³⁰ Yield: ~75%. The ^1H NMR spectrum is shown in Figure S1.

Synthesis of 7-(2-Hydroxyethoxy)-4-methylcoumarin. 7-Hydroxy-4-methylcoumarin (5.00 g, 0.0300 mol) was dissolved in 250 mL of acetone in a two-neck flask, followed by addition of K_2CO_3 (21.14 g, 0.1500 mol) and 2-bromoethanol (17.92 g, 0.1400 mol) under vigorous stirring. Then the suspension was transferred into the oil bath at $60\text{ }^\circ\text{C}$ and allowed to react under reflux with argon protection for 48 h. The reaction mixture was filtered to remove undissolved salts and evaporated to remove acetone under vacuum. The residue (yellowish solid) was dissolved in 500 mL of DCM and washed with 1.0 M NaOH ($2 \times 250\text{ mL}$) and DI water (250 mL) successively. The organic phase was dried over anhydrous MgSO_4 and evaporated under vacuum to remove DCM. The crude product (white solid) was then recrystallized from ethanol to yield white crystal. Yield: ~80%. The ^1H NMR spectrum is shown in Figure S2.

Synthesis of 7-(2-Methacryloyloxyethoxy)-4-methylcoumarin Monomer. 7-(2-Hydroxyethoxy)-4-methylcoumarin (2.00 g, 9.08 mmol) and TEA (2.220 g, 21.94 mmol) were dissolved in anhydrous THF (150 mL) in an ice bath. Methacryloyl chloride (1.200 g, 11.48 mmol) was first dissolved in 25 mL of anhydrous THF and added dropwise into the mixture over 1 h. After the addition of methacryloyl chloride, the ice bath was withdrawn and the mixture was kept stirring at ambient temperature for 36 h and finally quenched by adding 5.0 mL of MeOH. The mixture was filtered to remove TEA·HCl salt, and the solvent was removed via a rotary evaporator. The residue was redissolved in DCM (100 mL) and washed with DI water (200 mL) and saturated brine (200 mL) successively. The organic phase was dried over anhydrous MgSO_4 and evaporated under vacuum to remove the solvent to yield a yellowish solid. Purification with column chromatography (*n*-hexane/EtOAc, 4:1) gave 1.78 g of 7-(2-methacryloyloxyethoxy)-4-methylcoumarin

as a yellowish crystal. The ^1H NMR spectrum is shown in Figure S3. Yield: 65%.

Copolymerization of DEA and CMA by ATRP. A 25 mL flask with a rubber plug and a magnetic stirrer bar was charged with PEO-Br macroinitiator (0.300 g, $1.48 \times 10^{-1}\text{ mmol}$), PMDETA ($2.62 \times 10^{-2}\text{ g}$, $1.48 \times 10^{-1}\text{ mmol}$), DEA (2.74 g, 14.81 mmol), CMA ($4.27 \times 10^{-1}\text{ g}$, 1.48 mmol), and anisole (2.00 mL). Then the mixture was frozen and deoxygenated by flushing argon for 15 min before the addition of $\text{Cu}(\text{I})\text{Br}$ ($2.16 \times 10^{-2}\text{ g}$, $1.48 \times 10^{-1}\text{ mmol}$). The mixture was then sealed and emerged in an oil bath at $70\text{ }^\circ\text{C}$. The relative molar ratio of [PEO-Br]/[PMDETA]/[Cu(I)-Br]/[DEA]/[CMA] was 1:1:1:100:10. The reaction was polymerized for 24 h and terminated by cooling the solution to room temperature and exposing it to air. The polymer solution was diluted with DCM (150 mL), passed through a silica gel column for the removal of catalyst, and vacuum evaporated to yield a light brown, sticky solid. The crude product was finally lyophilized to yield PEO-*b*-P(DEA₉₄-stat-CMA₅) (yield: ~60%). The ^1H NMR spectrum is shown in Figure S4. The conversion of PEO-*b*-P(DEA-stat-CMA) is calculated to be ~88%, which is consistent with the GPC result shown in Figure S5. Calculation details of the degree of polymerization of PEO-*b*-P(DEA₉₄-stat-CMA₅) are discussed in Table S1.

Self-Assembly of PEO-*b*-P(DEA₉₄-stat-CMA₅) Diblock Copolymer into NEVs. NEVs were prepared according to the following protocol. As the nonsolvent of the P(DEA-stat-CMA) block, 10.0 mL of DI water was added dropwise to 5.0 mL of polymer solution in THF (6.8 mg/mL) over a period of 1 h under vigorous stirring. The residual THF was removed by dialyzing against DI water ($6 \times 500\text{ mL}$) for 2 days. The whole self-assembly procedure was conducted in the dark, preventing the photodimerization of coumarins. After being dialyzed, the obtained vesicles were characterized immediately by DLS and SLS to determine the hydrodynamic radius and the radius of gyration simultaneously on the same light-scattering device (ALV-5000).

Photo-Cross-Linking Procedure. A vial containing the polymer vesicle solution (1.67 mg/mL in DI water) was placed under a UV-vis spot curing system (8000 mw/cm²) at a λ of ~365 nm. The photo-cross-linking process was monitored by a UV-vis spectrometer at predetermined time intervals (Figure S7A). The dimerization degree, which reflects the cross-linking degree of polymer vesicles, is calculated from the change of UV absorbance at 320 nm defined as $1 - A_t/A_0$ (where A_0 is the initial absorbance at 320 nm and A_t is the absorbance after a certain irradiation time).⁵²

Preparation of Au Nanoparticle Decorated NEVs. To further visually display the coumarin-poor patches in the NEVs, we selectively decorated those patches with AuNPs. An aqueous HAUCl₄ solution was first added into a diluted NEV solution at a HAUCl₄/DEA molar ratio of 1:47, resulting in protonation of the tertiary amine groups of the DEA moiety followed by the incorporation of the counterion, AuCl_4^- . After stirring for 1 h, the succeeding *in situ* reduction of trivalent Au to zerovalent AuNPs was carried out via NaBH₄ solution (1:1 molar ratio relative to the amount of HAUCl₄ used). The NEV solution turned wine red immediately. Then the Au-decorated NEV solution was dialyzed against DI water to remove excess NaBH₄. When lyophilized and dispersed in THF, AuNP-loaded NEVs still stayed in an associated state according to the high count rate, suggesting that cross-linked NEVs were stable even in a highly reductive environment (NaBH₄ solution). Although AuNP decoration was exploited to distinguish phase-segregated regions, the acquired colloidal AuNPs have attracted increasing attention as recyclable synthetic catalysts for various organic reactions,⁵³ especially in the case of cross-linked NEVs (barely affected by the external physical and chemical disturbance). The D_h of aqueous AuNP-decorated NEVs (Figure S8a in the Supporting Information) was in good agreement with TEM observation.

Procedure for Encapsulating Glucose Oxidase and Hemoglobin into NEVs. GOx and Hb-loading into NEVs was performed according to the following protocol. Since the patches in the vesicle membranes are coumarin-poor regions that are pH-responsive, 3.00 mL of the preprepared mixture solution of NEVs, glucose oxidase, and hemoglobin (NEVs: 1.72 mg/mL;

glucose oxidase: 1.50 mg/mL; hemoglobin: 0.50 mg/mL) was tuned to pH 5.5 using HCl solution to solvate DEA segments (that is to say, open the valve) to favor the entrance of glucose oxidase and hemoglobin into the NEVs by osmotic pressure. The mixture was incubated at 25 °C for 2 days with stirring. After incubation the mixture was intentionally tuned to pH 6.5 to shut down the DEA valves and minimize physical adsorption between the NEVs and biomacromolecules caused by surface charge (Table S2), followed by purifying via SEC (size exclusion column containing Sepharose 4B) to remove unloaded biomacromolecules.⁴⁴ Then the size of the NEVs, the concentration of GOx and Hb inside the NEVs, and the BLE were evaluated and calculated by DLS and UV-vis spectroscopy (see Figure 7) with the pure NEV solution as the reference, which is very important because it will give a false high BLE if an incorrect reference is used. All the aliquots with a strong light-scattering intensity (high count rates) were collected and combined. The concentration of the NEV solution was calculated to be ca. 0.37 mg/mL, and the final concentration of hemoglobin was determined to be 0.022 mg/mL by monitoring the UV-vis absorbance at 404 nm (characteristic Soret absorbance peak of heme, Figure 7A, curve a) based on the hemoglobin calibration curve (see Figure 7D). The final concentration of glucose oxidase was determined to be 0.046 mg/mL by monitoring the UV-vis absorbance at 280 nm (Figure 7C) and subtracting the absorbance contributed by hemoglobin at this same wavelength.

Procedure for Encapsulating Fluorescently Labeled siRNA into NEVs. The encapsulation of fluorescently labeled siRNA was performed according to the following protocol. A 1.0 mL amount of the NEV solution (1.0 mg/mL) was mixed with 100.0 μL of preprepared siRNA solution (330.0 μg/mL). The mixture was then tuned to pH 4.0 using HCl solution for the protonation of DEA segments, favoring the entrance of siRNA into NEVs by osmotic pressure. The mixture was incubated at 25 °C for 24 h with stirring. After incubation, the mixture was intentionally tuned to neutral pH to close the DEA valves of NEVs, followed by purifying via SEC (size exclusion column containing Sepharose 4B) to remove unloaded siRNA.⁴⁴

Biocatalysis Procedure of Gox and Hb-Loaded NEVs. A 1.00 mL amount of enzyme-loaded NEV solution was mixed with 1.00 mL of o-phenylenediamine (OPD) solution at a concentration of 0.50 mg/mL (dissolved on-site) and 25.00 μL of glucose at a concentration of 85.8 mg/mL (dissolved on-site). During the catalytic process, glucose was first oxidized by glucose oxidase to form gluconic acid and H₂O₂. The latter then participated in the hemoglobin-catalyzing OPD oxidation to form 2,3-diaminophenazine (DAPN). Therefore, the mixture was monitored using a UV-vis spectrometer at 428 nm, which is the characteristic absorbance of DAPN in water. Reference samples, sample b (only GOx and Hb), sample c (only Hb), sample d (only NEVs), and sample e (only GOx), were also prepared accordingly.

Conflict of Interest: The authors declare no competing financial interest.

Acknowledgment. J.D. is supported by Shanghai 1000 Plan (SH01068), the program for professor of special appointment (Eastern Scholar) at Shanghai Institutions of Higher Learning (P2009011), National Natural Science Foundation of China (21174107 and 21374080), Ph.D. Program Foundation of Ministry of Education (20110072110048), Fok Ying Tong Education Foundation (132018), and the Fundamental Research Funds for the Central Universities.

Supporting Information Available: Scheme S1, Figures S1–S10, and Tables S1–S2 for the synthetic route, and GPC, NMR, UV-vis, and DLS results. This material is available free of charge via the Internet at <http://pubs.acs.org>.

REFERENCES AND NOTES

- Fried, H.; Kutay, U. Nucleocytoplasmic Transport: Taking an Inventory. *Cell. Mol. Life Sci.* **2003**, *60*, 1659–1688.
- Grunwald, D.; Singer, R. H.; Rout, M. Nuclear Export Dynamics of RNA-Protein Complexes. *Nature* **2011**, *475*, 333–341.
- Taddei, A.; Van Houwe, G.; Hediger, F.; Kalck, V.; Cubizolles, F.; Schober, H.; Gasser, S. M. Nuclear Pore Association Confers Optimal Expression Levels for an Inducible Yeast Gene. *Nature* **2006**, *441*, 774–778.
- D'Angelo, M. A.; Anderson, D. J.; Richard, E.; Hetzer, M. W. Nuclear Pores Form *de Novo* from Both Sides of the Nuclear Envelope. *Science* **2006**, *312*, 440–443.
- Fahrenkrog, B.; Koser, J.; Aeby, U. The Nuclear Pore Complex: A Jack of All Trades?. *Trends Biochem. Sci.* **2004**, *29*, 175–182.
- Stoffler, D.; Feja, B.; Fahrenkrog, B.; Walz, J.; Typke, D.; Aeby, U. Cryo-Electron Tomography Provides Novel Insights into Nuclear Pore Architecture: Implications for Nucleocytoplasmic Transport. *J. Mol. Biol.* **2003**, *328*, 119–130.
- Fahrenkrog, B.; Aeby, U. The Nuclear Pore Complex: Nucleocytoplasmic Transport and Beyond. *Nat. Rev. Mol. Cell Biol.* **2003**, *4*, 757–766.
- Stewart, C. L.; Roux, K. J.; Burke, B. Blurring the Boundary: The Nuclear Envelope Extends Its Reach. *Science* **2007**, *318*, 1408–1412.
- Terry, L. J.; Shows, E. B.; Wente, S. R. Crossing the Nuclear Envelope: Hierarchical Regulation of Nucleocytoplasmic Transport. *Science* **2007**, *318*, 1412–1416.
- Cui, H. G.; Chen, Z. Y.; Zhong, S.; Wooley, K. L.; Pochan, D. J. Block Copolymer Assembly via Kinetic Control. *Science* **2007**, *317*, 647–650.
- Pochan, D. J.; Chen, Z. Y.; Cui, H. G.; Hales, K.; Qi, K.; Wooley, K. L. Toroidal Triblock Copolymer Assemblies. *Science* **2004**, *306*, 94–97.
- Wang, X. S.; Guerin, G.; Wang, H.; Wang, Y. S.; Manners, I.; Winnik, M. A. Cylindrical Block Copolymer Micelles and Co-Micelles of Controlled Length and Architecture. *Science* **2007**, *317*, 644–647.
- Won, Y. Y.; Davis, H. T.; Bates, F. S. Giant Wormlike Rubber Micelles. *Science* **1999**, *283*, 960–963.
- Mitragotri, S.; Lahann, J. Physical Approaches to Biomaterial Design. *Nat. Mater.* **2009**, *8*, 15–23.
- Chen, W. Q.; Du, J. Z. Ultrasound and pH Dually Responsive Polymer Vesicles for Anticancer Drug Delivery. *Sci. Rep.* **2013**, *3*, DOI:10.1038/srep02162.
- Zhu, Y. Q.; Fan, L.; Yang, B.; Du, J. Z. Multifunctional Homopolymer Vesicles for Facile Immobilization of Gold Nanoparticles and Effective Water Remediation. *ACS Nano* **2014**, *8*, 5022–5031.
- Du, J. Z.; O'Reilly, R. K. Anisotropic Particles with Patchy, Multicompartment and Janus Architectures: Preparation and Application. *Chem. Soc. Rev.* **2011**, *40*, 2402–2416.
- Jeong, I. K.; Gao, G. H.; Li, Y.; Kang, S. W.; Lee, D. S. A Biodegradable Polymericosome with pH-Tuning On-Off Membrane Based on Poly(beta-amino ester) for Drug Delivery. *Macromol. Biosci.* **2013**, *13*, 946–953.
- Renggli, K.; Baumann, P.; Langowska, K.; Onaca, O.; Bruns, N.; Meier, W. Selective and Responsive Nanoreactors. *Adv. Funct. Mater.* **2011**, *21*, 1241–1259.
- Vriezema, D. M.; Comellas Aragonès, M.; Elemans, J. A. A. W.; Cornelissen, J. J. L. M.; Rowan, A. E.; Nolte, R. J. M. Self-Assembled Nanoreactors. *Chem. Rev.* **2005**, *105*, 1445–1490.
- Minten, I. J.; Hendriks, L. J. A.; Nolte, R. J. M.; Cornelissen, J. J. L. M. Controlled Encapsulation of Multiple Proteins in Virus Capsids. *J. Am. Chem. Soc.* **2009**, *131*, 17771–17773.
- Patterson, D. P.; Prevelige, P. E.; Douglas, T. Nanoreactors by Programmed Enzyme Encapsulation Inside the Capsid of the Bacteriophage P22. *ACS Nano* **2012**, *6*, 5000–5009.
- Griebelnow, K.; Klibanov, A. M. On Protein Denaturation in Aqueous–Organic Mixtures but Not in Pure Organic Solvents. *J. Am. Chem. Soc.* **1996**, *118*, 11695–11700.
- Ruysschaert, T.; Sonnen, A. F. P.; Haefele, T.; Meier, W.; Winterhalter, M.; Fournier, D. Hybrid Nanocapsules: Interactions of ABA Block Copolymers with Liposomes. *J. Am. Chem. Soc.* **2005**, *127*, 6242–6247.
- Kim, K. T.; Cornelissen, J. J. L. M.; Nolte, R. J. M.; van Hest, J. C. M. A Polymericosome Nanoreactor with Controllable Permeability Induced by Stimuli-Responsive Block Copolymers. *Adv. Mater.* **2009**, *21*, 2787–2791.

26. Chiu, H.-C.; Lin, Y.-W.; Huang, Y.-F.; Chuang, C.-K.; Chern, C.-S. Polymer Vesicles Containing Small Vesicles within Interior Aqueous Compartments and pH-Responsive Transmembrane Channels. *Angew. Chem., Int. Ed.* **2008**, *47*, 1875–1878.
27. Bellomo, E. G.; Wyrsta, M. D.; Pakstis, L.; Pochan, D. J.; Deming, T. J. Stimuli-Responsive Polypeptide Vesicles by Conformation-Specific Assembly. *Nat. Mater.* **2004**, *3*, 244–248.
28. Gao, C. Y.; Donath, E.; Mohwald, H.; Shen, J. C. Spontaneous Deposition of Water-Soluble Substances into Microcapsules: Phenomenon, Mechanism, and Application. *Angew. Chem., Int. Ed.* **2002**, *41*, 3789–3793.
29. Wang, F.; Feng, J.; Tong, W.; Gao, C. A Facile Pathway to Fabricate Microcapsules by *in situ* Polyelectrolyte Coacervation on Poly(styrene sulfonate)-Doped CaCO₃ Particles. *J. Mater. Chem.* **2007**, *17*, 670–676.
30. Du, J. Z.; Armes, S. P. pH-Responsive Vesicles Based on a Hydrolytically Self-Cross-Linkable Copolymer. *J. Am. Chem. Soc.* **2005**, *127*, 12800–12801.
31. Alber, F.; Dokudovskaya, S.; Veenhoff, L. M.; Zhang, W. H.; Kipper, J.; Devos, D.; Suprapto, A.; Karni-Schmidt, O.; Williams, R.; Chait, B. T.; et al. The Molecular Architecture of the Nuclear Pore Complex. *Nature* **2007**, *450*, 695–701.
32. Lu, Y.; Ballauff, M. Thermosensitive Core-Shell Microgels: From Colloidal Model Systems to Nanoreactors. *Prog. Polym. Sci.* **2011**, *36*, 767–792.
33. Christian, D. A.; Tian, A. W.; Ellenbroek, W. G.; Levental, I.; Rajagopal, K.; Janmey, P. A.; Liu, A. J.; Baumgart, T.; Discher, D. E. Spotted Vesicles, Striped Micelles and Janus Assemblies Induced by Ligand Binding. *Nat. Mater.* **2009**, *8*, 843–849.
34. Antonietti, M.; Bremser, W.; Schmidt, M. Microgels: Model Polymers for the Crosslinked State. *Macromolecules* **1990**, *23*, 3796–3805.
35. Baumann, F.; Deubzer, B.; Geck, M.; Dauth, J.; Sheiko, S.; Schmidt, M. Soluble Organosilicon Micronetworks with Spatially Confined Reaction Sites. *Adv. Mater.* **1997**, *9*, 955–958.
36. Cai, Y.; Tang, Y.; Armes, S. P. Direct Synthesis and Stimulus-Responsive Micellization of Y-Shaped Hydrophilic Block Copolymers. *Macromolecules* **2004**, *37*, 9728–9737.
37. Orlova, E. V.; Saibil, H. R. Structural Analysis of Macromolecular Assemblies by Electron Microscopy. *Chem. Rev.* **2011**, *111*, 7710–7748.
38. Huang, J.; Bonduelle, C.; Thevenot, J.; Lecommandoux, S.; Heise, A. Biologically Active Polymersomes from Amphiphilic Glycopeptides. *J. Am. Chem. Soc.* **2012**, *134*, 119–122.
39. Rybtchinski, B. Adaptive Supramolecular Nanomaterials Based on Strong Noncovalent Interactions. *ACS Nano* **2011**, *5*, 6791–6818.
40. Hunter, C. A.; Sanders, J. K. M. The Nature of π-π Interactions. *J. Am. Chem. Soc.* **1990**, *112*, 5525–5534.
41. Hirano, A.; Arakawa, T.; Shiraki, K. Arginine Increases the Solubility of Coumarin: Comparison with Salting-in and Salting-out Additives. *J. Biochem.* **2008**, *144*, 363–369.
42. Wang, J.; Gu, J. D.; Leszczynski, J. The Electronic Spectra of the Sandwich Stacked PFBT: A Theoretical Study. *J. Phys. Chem. A* **2011**, *115*, 6376–6382.
43. Yan, Q.; Yuan, J.; Cai, Z.; Xin, Y.; Kang, Y.; Yin, Y. Voltage-Responsive Vesicles Based on Orthogonal Assembly of Two Homopolymers. *J. Am. Chem. Soc.* **2010**, *132*, 9268–9270.
44. Wang, L.; Chierico, L.; Little, D.; Patikarnmonthon, N.; Yang, Z.; Azzouz, M.; Madsen, J.; Armes, S. P.; Battaglia, G. Encapsulation of Biomacromolecules within Polymersomes by Electroporation. *Angew. Chem., Int. Ed.* **2012**, *51*, 11122–11125.
45. Wolf, H.; Rols, M. P.; Boldt, E.; Neumann, E.; Teissie, J. Control by Pulse Parameters of Electric Field-Mediated Gene-Transfer in Mammalian-Cells. *Biophys. J.* **1994**, *66*, 524–531.
46. Ho, S. Y.; Mittal, G. S. Electroporation of Cell Membranes: A Review. *Crit. Rev. Biotechnol.* **1996**, *16*, 349–362.
47. Liu, Y.; Du, J. J.; Yan, M.; Lau, M. Y.; Hu, J.; Han, H.; Yang, O. O.; Liang, S.; Wei, W.; Wang, H.; et al. Biomimetic Enzyme Nanocomplexes and Their Use as Antidotes and Preventive Measures for Alcohol Intoxication. *Nat. Nanotechnol.* **2013**, *8*, 187–192.
48. Wang, Q. G.; Yang, Z. M.; Zhang, X. Q.; Xiao, X. D.; Chang, C. K.; Xu, B. A Supramolecular-Hydrogel-Encapsulated Hemin as an Artificial Enzyme to Mimic Peroxidase. *Angew. Chem., Int. Ed.* **2007**, *46*, 4285–4289.
49. Qi, W.; Yan, X.; Duan, L.; Cui, Y.; Yang, Y.; Li, J. Glucose-Sensitive Microcapsules from Glutaraldehyde Cross-Linked Hemoglobin and Glucose Oxidase. *Biomacromolecules* **2009**, *10*, 1212–1216.
50. Zhang, K.; Mao, L. Y.; Cai, R. X. Stopped-Flow Spectrophotometric Determination of Hydrogen Peroxide with Hemoglobin as Catalyst. *Talanta* **2000**, *51*, 179–186.
51. Sun, H.; Hu, N. F.; Ma, H. Y. Direct Electrochemistry of Hemoglobin in Polyacrylamide Hydrogel Films on Pyrolytic Graphite Electrodes. *Electroanalysis* **2000**, *12*, 1064–1070.
52. Jiang, J.; Qi, B.; Lepage, M.; Zhao, Y. Polymer Micelles Stabilization on Demand through Reversible Photo-Cross-Linking. *Macromolecules* **2007**, *40*, 790–792.
53. Ley, S. V.; Ramarao, C.; Gordon, R. S.; Holmes, A. B.; Morrison, A. J.; McConvey, I. F.; Shirley, I. M.; Smith, S. C.; Smith, M. D. Polyurea-Encapsulated Palladium(II) Acetate: A Robust and Recyclable Catalyst for Use in Conventional and Super-critical Media. *Chem. Commun.* **2002**, 1134–1135.